It's a gas: Oxidative dehydrogenation of propane over boron nitride catalysts

Peter Kraus[a]*, R. Peter Lindstedt[b]

a) School of Molecular and Life Sciences,
Curtin University,
GPO Box U1987, Perth 6845, WA

b) Department of Mechanical Engineering,
Imperial College London,
Exhibition Road, London SW7 2AZ

Abstract

Boron nitride and related boron-containing materials have recently been suggested as very promising catalysts in the oxidative dehydrogenation of propane. The high selectivity towards propylene at comparably high conversion significantly exceeds the performance of established vanadium-based catalysts. In the current work we show that the high selectivity towards propylene and ethylene is fully consistent with a gas-phase conversion mechanism and that it can be modelled reasonably well by the recent detailed microkinetic reaction mechanism of Hashemi and coworkers. Our analysis, using five hypothetical limit heterogeneous mechanisms, also shows that the boron nitride catalyst is responsible for initiating the gas-phase chemistry. Experimental C_2:C_1 product ratios with an undiluted catalytic bed can be reproduced by incorporating C–C bond scission into the surface mechanism. The trends in the selectivities of minor species upon dilution of the catalytic bed observed by Venegas and Hermans are here explained as gas-phase phenomena. The current work also highlights the importance of modelling of the complete heated zone, including the rear heat shields and padding of the reactor if present.

1 Introduction

"It is surprising that boron nitride (BN), a material known for its high stability under oxidative conditions, is catalytically active at all." [1] Since this landmark 2016 publication by Grant et al. [1] in Science, boron-containing materials have become a hot topic in oxidative dehydrogenation (ODH) and with good reason. The claimed selectivity to propylene ($S(C_3H_6)$) is 80% at propane conversion ($X(C_3H_8)$) of 21%, [2] while established vanadium-based catalysts offer only 60% selectivity at half the conversion. [1,3]

*E-mail: peter.kraus@curtin.edu.au

The performance of some BN materials remains stable up to 300 hours on stream[2] and catalysts can be regenerated by co-feeding NH_3.[4] In fact, it seems good ODH performance can be obtained with any material provided it contains boron.[5,6]

Despite the high temperatures required, usually in excess of 500°C, surprisingly little attention has been paid to gas-phase kinetics. Blank experiments with SiO_2 instead of BN in the reactor show almost no conversion.[4,7] However, the operating conditions across the various catalytic tests have not been standardised,[8] making comparisons between datasets difficult. Pretreatment, heat transport, diluent and dilution, and reactor dimensions all play a significant role in the activity of hexagonal boron nitride (hBN).[6,8]

It is a fortunate coincidence that a revised, "low-temperature" (from a combustion point of view) gas phase mechanism for propane oxidation has been recently published.[9] This allows us to investigate the relative gas-phase and catalytic contributions to the observed ODH of propane. We attempt to explain the differences between the predicted gas-phase behaviour and observed catalytic performance data[8] by coupling a heterogeneous model to the revised gas-phase chemistry of Hashemi et al.[9] We investigate the plausibility of five heterogeneous "limit" mechanisms, derived from literature, and incorporate C–C scission pathways to form a heterogeneous model comprising 23 reactions. The reference experimental conditions span a range of residence times and consider the impact of dilution of the catalyst.

2 Computational methods

The gas-phase and heterogeneous modelling in this work was performed using Cantera version 2.4.[10] All fitting is performed with the nonlinear least squares routine `curve_fit` from the `scipy.optimize` Python library. The inputs used in the modelling, the resulting data, and the post-processing routines are all included in the Binder-compatible Supporting Information archive.

2.1 Gas-phase modelling

Two gas-phase models are used in this work: i) a recent detailed combustion model developed for high-pressure oxidation of propane (denoted the "DTU" model in the following),[9] and ii) an older model developed for high-temperature combustion of jet fuel surrogate mixtures (denoted "JetSurF" in the

following).[11] The DTU model includes low-temperature chemistry of the hydroperoxyalkyl (QOOH) radicals,[12] as well as revised C_3H_8 thermal activation[13] and radical abstraction[9,14] rates. By comparison, the JetSurF model is based on an older C_1-C_4 submechanism,[15] that was extensively validated for higher temperatures.

The ignition delay and selectivity-vs-conversion plots shown in Section 3 are modelled using an adiabatic constant pressure reactor, with an initial time step of 10^{-10} s and a largest time step of 10^{-5} s. The ignition point τ is determined as the time corresponding to the maximum in the time derivative of the OH concentration ($\tau = \texttt{arg max}\ f(t) := d[\mathrm{OH}]/dt$).

2.2 Heterogeneous modelling

Table 1: Heterogeneous H/O sub-mechanism.[16] $\theta(X)$ is surface fraction of species X, s_0 is the sticking coefficient.

Pathway	**Reaction equation**	**Pre-exponential** A (m, mol, s)	**T-dependency** β (–)	**Barrier** E_A (kJ/mol)
R1	$H_2 + 2^{\dagger}Bs \rightarrow 2\ Hs$	4.4579×10^4	0.5	0
R2	$2\ Hs \rightarrow H_2 + 2\ Bs$	3.7×10^{15}	0	67.4 - 6×θ(Hs)
R3	$H + Bs \rightarrow Hs$	$s_0 = 1$	0	0
R4	$O_2 + 2\ Bs \rightarrow 2\ Os$	1.8×10^9	-0.5	0
R5	$O_2 + 2\ Bs \rightarrow 2\ Os$	$s_0 = 0.023$	0	0
R6	$2\ Os \rightarrow O_2 + 2\ Bs$	3.7×10^{15}	0	213.2 - 60×θ(Os)
R7	$O + Bs \rightarrow Os$	$s_0 = 1$	0	0
R8	$H_2O + Bs \rightarrow H_2Os$	$s_0 = 0.75$	0	0
R9	$H_2Os \rightarrow H_2O + Bs$	1×10^{13}	0	40.3
R10	$OH + Bs \rightarrow OHs$	$s_0 = 1$	0	0
R11	$OHs \rightarrow OH + Bs$	1×10^{13}	0	192.8
R12	$Hs + Os \leftrightarrow OHs + Bs$	3.7×10^{15}	0	11.5
R13	$Hs + OHs \leftrightarrow H_2Os + Bs$	3.7×10^{15}	0	17.4
R14	$OHs + OHs \leftrightarrow H_2Os + Os$	3.7×10^{15}	0	48.2

†: first order in rate law.

As a base for the heterogeneous model, we use the H/O sub-mechanism (14 reactions and thermochemistry) from a CH_4 oxidation model developed for platinum,[16] see Table 1. The choice is one of convenience as the mechanism is distributed with Cantera. Most pre-exponential factors in the sub-mechanism are order-of-magnitude estimates (10^{13} s^{-1} for desorptions and 3.7×10^{15} $m^3mol^{-1}s^{-1}$ for bimolecular surface reactions). The sub-mechanism is numerically efficient due to its small size. All parameters are retained from the original mechanism, with the exception of the site density, which has been

fitted to match the observed conversion. The sensitivities to the site density (Γ) and oxygen adsorption parameters are assessed below. The thermochemistry of additional surface species is estimated from the corresponding gas-phase species in the DTU mechanism without further correction. In our previous work on Pt and Rh, the thermochemistry of the surface species was corrected by the heat of adsorption of the gas-phase species, obtained from systematic semi-empirical estimates.[17] Similar corrections for hBN would require values for the atomic heats of adsorption, which are currently unavailable and would have to be estimated. As a result, we introduced irreversible catalytic reaction steps (i.e. separate forward and reverse reactions) for the $C_3/C_2/C_1$ surface chemistry.

Table 2: Properties of materials used in the heterogeneous model.

Material	**Thermal cond.** κ (W m^{-1}K^{-1})	**Bulk density** ρ (kg m^{-3})	**Surface area** S_A (m^{2}kg^{-1})
SiO_2	3[18]	100	1000
hBN	33[8]	410[8]	7000[8]
SiC	300[19]	860[20]	13000[20]

The catalytic reactor is modelled using a plug flow approximation, with the modelled domain comprising four sections: a SiO_2-wool heat shield, a catalytic section filled with hBN or optionally diluted with SiC, another SiO_2-wool heat shield, and the remainder of the reactor filled with SiO_2 chips. The applied boundary conditions are taken from Venegas and Hermans where available:[8] an inlet temperature of 298 K; bath temperature of 773 K; reactor radius r of 4 mm; the tortuosity of the catalytic and SiO_2-wool sections set to 4; a porosity of the catalytic and SiO_2-wool sections of 0.4; inlet flow rates between 40 and 160 ml min^{-1}; length of the front and rear SiO_2-wool sections of 15 and 10 mm, respectively; length of the catalytic section between 3 and 25.5 mm depending on dilution of hBN with SiC; an overall reactor length of 200 mm. The inlet composition is 30% C_3H_8, 15% O_2, and 55% N_2 by volume in all cases. The porosity and tortuosity of the section containing SiO_2 chips is not provided; for simplicity we assume a tortuosity of 1 with the effect of porosity on conversion discussed below. The heat bath outside the modelled reactor is implemented as an isothermal bath. The bath is coupled to the active zone of the reactor using a $d = 4$ mm thick wall, properties of which depend on the material (see Table 2). The thermal conductances U_i for each reactor section i filled with material X are calculated according to Eq. (1), where V_i is the volume of the ith section.

$$U_i = \kappa_i(\mathrm{X}) \times d/(V_i S_{A_i}(\mathrm{X})\rho_i(\mathrm{X})) \tag{1}$$

$$A_{c_i} = V_i S_{A_i}(\mathrm{hBN})\rho_i(\mathrm{hBN})/f_{\mathrm{dil}} \tag{2}$$

The gas-phase chemistry is evaluated in all parts of the reactor, the heterogeneous mechanism is enabled only in the catalytic section. In cases where hBN is diluted by SiC, the catalytic area of each cell A_{c_i} is scaled down by the dilution factor $f_{\mathrm{dil}} = V_{\mathrm{bed}}/V_{\mathrm{cat}} \in \{1.0, 1.5, 2.0, 3.5, 6.0, 8.5\}$ (see Eq. (2)), and the thermal conductance is approximated as the weighted sum of the conductivities of hBN and SiC. The density of grid points i in the four sections of the modelled reactor is 10/mm for the front and rear SiO_2-wool sections, 50/mm for the hBN-containing section, and 1/mm for the section filled with SiO_2 chips. The grid resolution independence was confirmed using a 10× finer grid. With the basic grid resolution, the conversion is converged to within 6% of the finer grid value and selectivities to within 1%.

The carbon-based selectivities S and propane conversions X reported in this work are product based, using Eqs. (3) and (4), respectively.

$$S(\mathrm{prod}) = \frac{n_{\mathrm{C}}(\mathrm{prod})x(i,\mathrm{prod})f_e(i)}{\sum_{\mathtt{p}\neq \mathrm{C_3H_8}} n_{\mathrm{C}}(\mathtt{p})x(i,\mathtt{p})f_e(i)} \tag{3}$$

$$X(\mathrm{C_3H_8}) = \frac{\sum_{\mathtt{p}\neq \mathrm{C_3H_8}} n_{\mathrm{C}}(\mathtt{p})x(i,\mathtt{p})f_e(i)}{\sum_{\mathtt{r}} n_{\mathrm{C}}(\mathtt{r})x(i,\mathtt{r})f_e(i)} \tag{4}$$

Here, $n_{\mathrm{C}}(\mathtt{p})$ is number of carbon atoms in species $\mathtt{p}$, $x(i,\mathtt{p})$ is the mole fraction of $\mathtt{p}$ in cell i, and $f_e(i)$ is the expansion factor defined as $f_e(i) = x(i,\mathrm{N_2})/x(0,\mathrm{N_2})$. Note that the index $\mathtt{p}$ runs over the products only, while the index $\mathtt{r}$ runs over all species.

3 Results and discussion

To provide background for the catalytic aspects of the studied system, we will first investigate the behaviour of the gas-phase as predicted by the DTU and JetSurF combustion models under the experi-

mental boundary conditions. Then, we will assess the effect the surface chemistry of hBN could have on the selectivity of the overall system by using five hypothetical heterogeneous mechanisms. These limit mechanisms are intended to probe the extremes of catalytic behaviour in the context of the gas-phase chemistry. Finally, we attempt to reconcile the gas-phase effects with the limits of possible catalytic behaviour to try and match the observed conversion and selectivities.[8]

3.1 Gas-phase ignition

The temperatures used in most investigations of propane ODH over hBN, usually in excess of 500°C, are higher than the usual conditions applied with vanadium-based catalysts.[3] Despite this, the contribution of gas-phase chemistry to the performance of hBN has been largely ignored. Control experiments performed using a reactor filled only with quartz chips were reported, with "negligible" conversion well below 1%.[8] The only investigation where the gas-phase behaviour was assessed using a microkinetic model was the study of Loiland et al.,[21] however the choice of boundary conditions used by the authors is incongrous with the geometry of the experimental reactor.

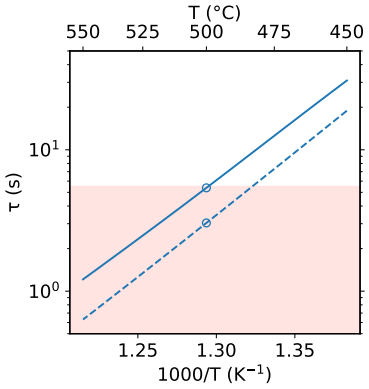

Figure 1: Adiabatic ignition delay τ of a 15% O_2, 30% C_3H_8, 55% N_2 mixture as a function of the initial temperature at atmospheric pressure. The DTU mechanism (——) is compared to the JetSurF mechanism (- - -). The red area indicates τ for the reactor in the experiments of Venegas and Hermans.[8] Circles highlight a temperature of 500°C.

The ignition delay shown in Fig. 1 presents an indication that gas-phase phenomena may play a non-negligible role under the studied conditions. At 500°C, the DTU mechanism (——) shows an ignition delay just outside the residence time domain in the experiments of Venegas and Hermans[8] (red zone); the JetSurF mechanism (- - -) predicts faster ignition. The experimental temperature of 500°C

is determined from a single thermocouple embedded in the catalytic bed,[8] and despite best practices ensuring the bed is as isothermal as practicable, small inhomogeneities from the reaction temperature would have an exponential effect on the kinetics this close to self-ignition.

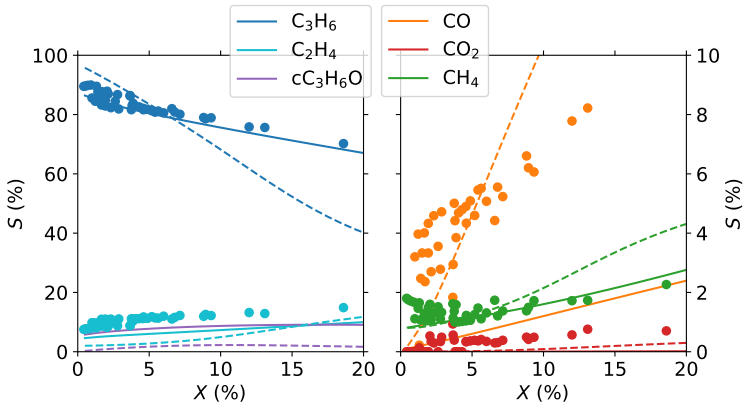

Figure 2: Selectivity vs conversion plot from gas-phase kinetics. The DTU mechanism (—) is compared to the JetSurF mechanism (- - -) and experimental data at all dilutions (•).[8] Modelled using an adiabatic reactor, with initial conditions of 500°C and atmospheric pressure, and a 15% O_2 / 30% C_3H_8 / 55% N_2 inlet composition.

The performance of hBN (and other B-containing materials) for ODH of propane is remarkable mainly due to the high selectivity to propylene and ethylene. However, as shown in Figure 2, the high selectivity to both propylene (—) and ethylene (—) is consistent with the kinetics of the DTU gas-phase mechanism. One major product predicted by the DTU mechanism but not observed experimentally is propylene oxide (cC_3H_6O, —).[8] For minor products, methane (—) is well predicted by the DTU mechanism, but the two combustion products CO_2 (- - -) and CO (- - -) are better captured by JetSurF. The results indicate strongly that the pyrolysis part of the DTU mechanism is accurate, while the low temperature oxidation behaviour is arguably questionable. The DTU mechanism contains revised propylene oxide formation rates via the QOOH route,[12] but it is a mechanistic dead end without destruction pathways. JetSurF contains destruction pathways via both ring opening towards acetone ($CH_3C(O)CH_3$) and propionaldehyde (CH_3CH_2CHO), as well as C–C bond scission pathways towards C_1+C_2 products. The DTU mechanism may be overpredicting the formation of propylene oxide, as shown by direct comparison to the JetSurF results (- - -). On the other hand, as propylene oxide is a liquid at room temperature and pressure, and the reactor effluent is cooled to -5°C to remove water prior to the chromatographic analysis, a significant part of propylene oxide may be inadvertently removed from

the effluent stream. The reported error in the experimental carbon mass balance is 3%,[8] significantly less than the amount of propylene oxide predicted by the DTU mechanism. Inclusion of decomposition pathways of propylene oxide into the gas-phase model should ultimately lead to increased CO_2 and CO production,[22] improving the agreement with available experimental data.

3.2 Catalytic sensitivity to porosity, site density, and O_2 adsorption

The value of the porosity of the reactor affects the residence time in the overall reactor. We apply the literature values of porosity[8] in the first three sections of the reactor. To estimate the effects of porosity of the last section on the overall conversion, we consider a two-step extension of the heterogeneous model shown in Table 1,

$$\begin{aligned}
&\mathrm{M1-R15}: \mathrm{C_3H_8} + 2\ \mathrm{B}s \rightarrow \mathrm{C_3H_7}s + \mathrm{H}s, \quad && A = 7.58706 \times 10^{-4}\ \mathrm{m^3 mol^{-1} s^{-1}}, && \beta = 0.5, && E_A = 0 \\
&\mathrm{M1-R16}: \mathrm{C_3H_7}s \rightarrow \mathrm{C_3H_6} + \mathrm{H}s, && A = 1 \times 10^{13}\ \mathrm{s^{-1}}, && \beta = 0, && E_A = 0
\end{aligned}$$

coupled to the DTU gas-phase mechanism. The conversion reported in the control experiments without hBN is $X(\mathrm{C_3H_8}) = 0.3\%$ at 500°C and 1% at 550°C,[8] this value is indicated in Figure 3 as ∘. This level of conversion is only matched when the porosity of the rear section is as low as 1%, which would be an unusually low value given the porosity of the SiO_2 wool is 40%[8] and the porosity of SiO_2 chips has been reported as high as 50%.[23] In the following, we apply an intermediate value of porosity of 20%, corresponding to a conversion of 0.9% in the control experiment. The desorption in M1-R16 is unlikely to be barrierless, however setting a barrier height has no effect as there is no alternative branch for $\mathrm{C_3H_7}s$ in the mechanism. The pre-exponential of M1-R15 can then be fitted to match the observed conversion.

However, in addition to the porosity of the last section of the reactor and the adsorption rate constant M1-R15, $X(\mathrm{C_3H_8})$ is also a function of the site density Γ. The physical constraint on the site density of hBN is $\Gamma \leq 3.04 \times 10^{-5}$ mol m^{-2}, derived from a theoretical unit cell area of 5.462 Å^2 per boron site.[24] The Γ used throughout the current work is fitted together with the pre-exponential of M1-R15 to ensure $X(\mathrm{C_3H_8}) = 3.65\%$ for the undiluted case, and 18.60% for $V_{\mathrm{bed}}/V_{\mathrm{cat}} = 8.5$, given porosity

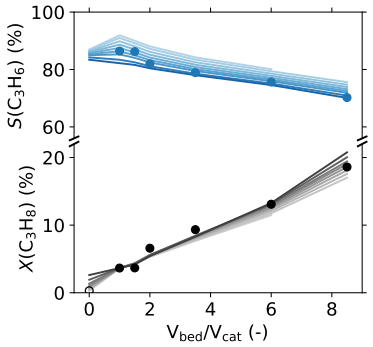

Figure 3: Effect of porosity on the propane conversion and propylene selectivity, with the pre-exponential of R15-1 fitted to match conversion for undiluted case. Shading implies porosity in the range of 1–50%. Γ set to 1.497×10^{-7} mol m^{-2} for all dilutions and porosities. Flow rate $\sim$ 40 ml min^{-1}.

of 20% in the last section of the reactor, shown in Figure 3. The resulting values are $A_{\mathrm{M1-R15}} = 7.58706 \times 10^{-4}$ m^{3}mol^{-1}s^{-1} and $\Gamma = 1.497 \times 10^{-7}$ mol m^{-2} corresponding to 5% availability of boron sites with respect to the the theoretical maximum. The dissociative adsorption described by M1-R15 can alternatively be thought of as a collision–sticking process, with a sticking coefficient $s_0 \sim 10^{-12}$. This is a very low value, especially when compared to the near-unity s_0's of H, O, and OH in Table 1, as well as the $s_0 = 5.8 \times 10^{-3}$ for C_3H_8 on rhodium.[25] To obtain the same rate constant at 500°C with a hypothethical propane s_0 of unity, the adsorption would have to proceed with a barrier of 180 kJ/mol. Alternatively, with a $s_0 = 5.8 \times 10^{-5}$, i.e. sticking 100× less likely than on Rh, the adsorption barrier would have to be 117 kJ/mol. Both barriers are very high, but well below the reported experimental apparent activation energies for ODH of propane (184–233 kJ/mol[2,21]). For comparison, on vanadium oxides, dissociative adsorption of propane was calculated to proceed with a barrier of 144–151 kJ/mol.[26] It is therefore much more likely the true propane activation process is at least two-step, including a reversible C_3H_8 adsorption, followed by a C–H bond activation on the surface with an appreciable barrier.

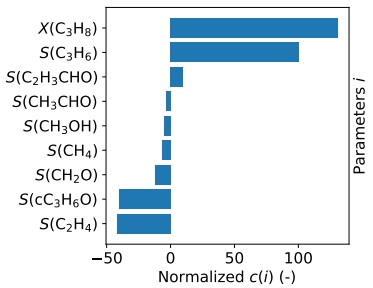

Figure 4: Normalised sensitivity coefficients $c(i)$ of parameters i with respect to the O_2 adsorption rate (R4).

The reaction parameters of the H/O submechanism are taken verbatim from Deutschmann et al.[16] As the original mechanism was developed for Pt, and we have adjusted Γ, a sensitivity analysis to the rate of O_2 adsorption (R4) by varying A_{R4} by an order of magnitude between $1.8 \times 10^8 - 1.8 \times 10^{10}$ $m^6 mol^{-2} s^{-1}$ is carried out. The absolute sensitivity coefficients $c(i) = \partial i(A_{R4})/\partial A_{R4}$ are smaller than 10^{-22}, indicating a very small sensitivity. The normalised coefficients of the 10 most sensitive parameters i are shown in Figure 4: both $X(C_3H_8)$ and $S(C_3H_6)$ correlate positively with A_{R4}. In a rigorous approach to mechanism development, the H/O submechanism would have to be tailored to account for the differences between Pt and hBN. Figure 4 shows that a further increase in the ratio of the effective sticking probabilities of O_2 and C_3H_6 would lead to a higher selectivity to propylene and a higher conversion. However, experimental oxygen and hydrogen selectivity data are currently not available for hBN, therefore the rates cannot be fitted, and would have to be determined ab initio.

Table 3: The five heterogeneous "limit" submechanisms.

Pathway	**Reaction equation**	**Pre-exponential** A (m, mol, s)	**T-dependency** β (–)	**Barrier** E_A (kJ/mol)
M1-R15	$C_3H_8 + 2\,Bs \rightarrow C_3H_7s + Hs$	† 7.58706×10^{-4}	0.5	0
M1-R16	$C_3H_7s \rightarrow C_3H_6 + Hs$	1×10^{13}	0	0
M2-R15	$C_3H_8 + 2\,Os \rightarrow C_3H_7Os + OHs$	† 6.18110×10^{-7}	0.5	0
M2-R16	$C_3H_7Os \rightarrow C_3H_6 + OHs$	1×10^{13}	0	0
M3-R15	$C_3H_8 + 2\,Os \rightarrow C_3H_7Os + OHs$	† 3.65604×10^{-7}	0.5	0
M3-R16i	$C_3H_7Os \rightarrow iC_3H_7O + Bs$	2×10^{13}	0	20.9
M3-R16n	$C_3H_7Os \rightarrow nC_3H_7O + Bs$	6×10^{13}	0	3.4
M4-R15	$C_3H_8 + 2\,Bs \rightarrow C_3H_7s + Hs$	† 5.02585×10^{-4}	0.5	0
M4-R16i	$C_3H_7s \rightarrow iC_3H_7 + Bs$	2×10^{13}	0	31.4
M4-R16n	$C_3H_7s \rightarrow nC_3H_7 + Bs$	6×10^{13}	0	20.9
M5-R15	$C_3H_8 + 2\,Os \rightarrow C_3H_7Os + OHs$	† 3.49928×10^{-7}	0.5	0
M5-R16	$C_3H_7Os \rightarrow C_2H_4 + CH_3 + Os$	1×10^{13}	0	0

†: fitted to obtain $X(C_3H_8) = 3.65\%$ with $\Gamma = 1.497 \times 10^{-7}$ mol m^{-2} and 20% porosity with undiluted catalyst at 40 ml min^{-1} flow.

3.3 Catalysis in the propylene forming limit

The first two of the limit mechanisms considered in this study are: M1: a direct propylene (C_3H_6) forming mechanism, and M2: an O*s*–mediated C_3H_6 forming mechanism. The latter has been proposed by Shi et al.[7] and is consistent with the presence of surface oxygen in X-ray photoelectron spectra (XPS)[1,5] as well as B–OH vibrations in infrared spectra.[7,27] We include the former to compare a direct adsorption

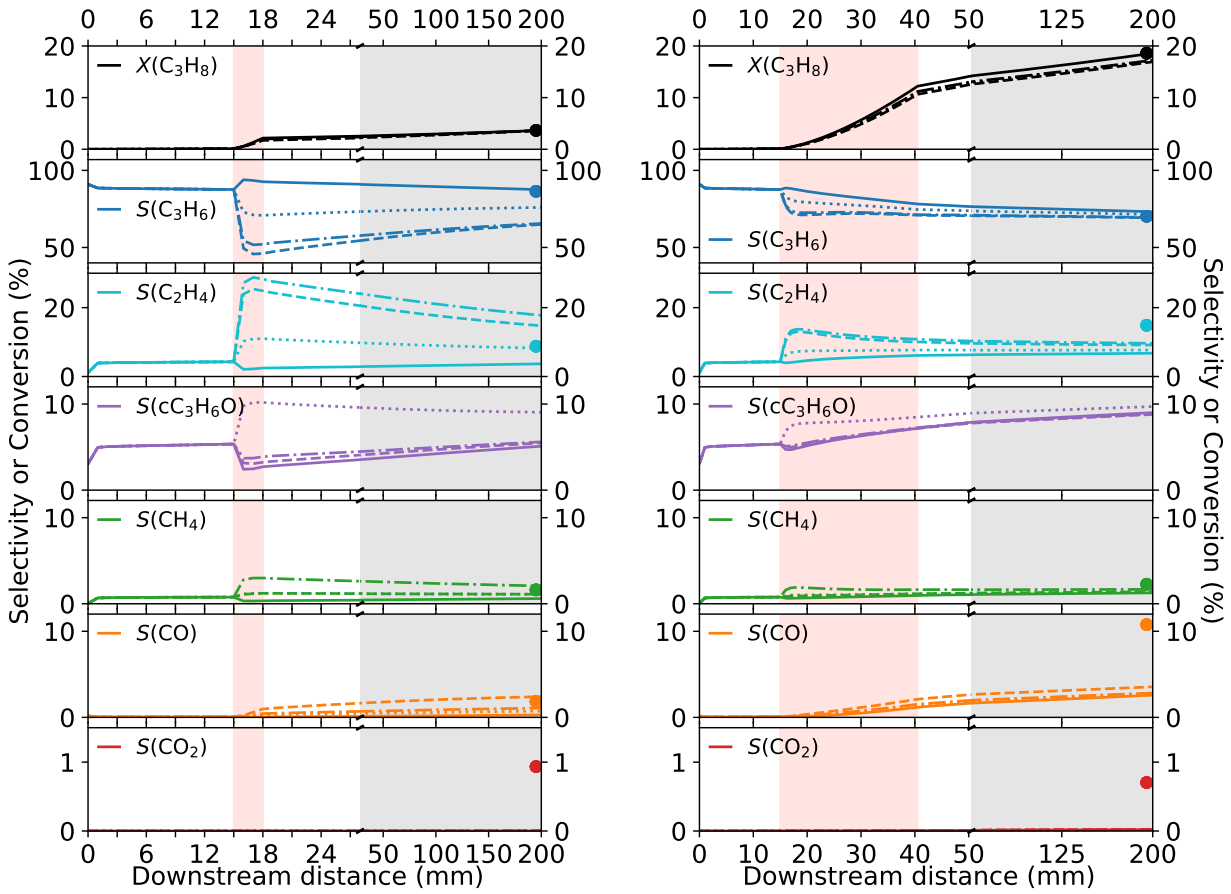

Figure 5: Selectivity and conversion of selected species as a function of downstream distance with four of the five limit mechanisms: M1: direct C_3H_6 (——), M3: Os-mediated xC_3H_7O (- - -), M4: direct C_3H_7 (·····), and M5: Os-mediated C–C scission (-·-·). Case with an undiluted catalyst (left) and with the highest dilution ($V_{bed}/V_{cat} = 8.5$, right), both at $\sim$ 40 ml min^{-1}. Lines are calculated data, circles are experimental results,[8] shaded areas correspond to the front and rear heat shield (white), the catalytic zone (red), and SiO_2 chips (gray).

pathway to the latter Os–mediated Eley-Rideal process. The rate constants are listed in Table 3.

Both the direct (—— in Fig. 5) and Os-mediated (not shown) C_3H_6 mechanisms show nearly identical selectivity and conversion profiles, despite the different nature of C_3H_8 activation on the catalytic surface. The availability of free and Os sites is therefore not limiting in the current model, with predicted surface coverages of Bs and Os of 1.8% and 98.2% after the first mm and 2.8% and 97.1% after the last mm of the undiluted catalyst, respectively. A small proportion of sites (0.06% in undiluted, 0.1% in diluted cases) is covered by OHs, regardless of the adsorption pathway. The presence of OHs is consistent with analysis of the spent catalysts, but it is not a conclusive proof of an Eley-Rideal mechanism, as the adsorption of propane may equally plausibly proceed on exposed Bs or Os sites, and the B–OH species

can be explained by either abstraction of the second H by Os leading to C_3H_6 formation, or by a surface reaction between Hs and Os. The predicted surface coverages may change once multiple branching pathways are introduced, and once the H/O submechanism is validated for hBN. The pre-exponentials of the adsorption steps in the two mechanisms differ by a factor of $\sim \times 10^3$ with the Os-mediated mechanism being the more active one. Considering the ratio of surface coverages at the front end of the catalytic section, this corresponds to an Eley-Rideal reaction-class "penalty" of 2/5 to achieve the same conversion as the direct dissociative adsorption pathway.

In the undiluted case, the two C_3H_6 mechanisms are unsurprisingly the most selective towards C_3H_6 (—) of the five. The downstream profiles show only a small amount of post-catalytic combustion of the main product (gray shading). However, the selectivity to minor species, and especially towards C_2H_4 (—), is significantly underpredicted by both mechanisms. Therefore, while C_3H_6 may be produced on the surface, it is unlikely to be the only catalytic product as proposed by Shi et al.[7] Upon dilution, the increase in conversion and decrease in $S(C_3H_6)$ is well captured. Both mechanisms underpredict $S(C_2H_4)$ as well as $S(CO)$ (—) by $\sim 8\%$. This may be a consequence of the high selectivity towards propylene oxide (cC_3H_6O, — , 9.0%), acrolein (C_2H_3CHO, 3.3%) and formaldehyde (CH_2O, 1.9%), neither of which has been observed experimentally.

3.4 Catalysis in the radical forming limit

The initially proposed mechanism for the activity of hBN (M3) involves an adsorption on oxygen-covered boron sites and leading to the formation of propoxy radicals (xC_3H_7O).[1] Here, we also consider the direct, propyl radical (xC_3H_7) forming analogue (M4). It is hard to imagine a catalytic process where propyl radicals would desorb from the surface rather than undergo further H-abstraction towards propylene. We include the propyl forming mechanism to probe the effects additional propyl radicals would have on the gas-phase behaviour, rather than as a proposed catalytic pathway. The rate constants are listed in Table 3. The pre-exponentials for the branching reactions to iso- and n-propoxy (or propyl) radicals are scaled 2:6 to account for the number of equivalent hydrogens in propane, and the barrier heights in desorption of the products are taken from the most similar gas-phase reactions in the DTU mechanism. Rather than overfitting the models by fitting up to 6 parameters in each of the two

mechanisms, we have opted to fit only the adsorption pre-exponentials (M3-R15, M4-R15), and use order of magnitude estimates for the other pre-exponentials and estimates for barriers from the gas-phase to define the branching ratios. As the reference experiments have been carried out at a single temperature, the choice of barrier heights is somewhat arbitrary.

The two mechanisms show a very different behaviour compared to the propylene forming limit (M1, M2), as well as with respect to each other. In the undiluted case, the propoxy mechanism (- - -) results in a significantly higher amount of C–C scission than the propyl mechanism (·····). The selectivity to the main product C_3H_6 is significantly underpredicted by both of these mechanisms, with selectivity to propylene dropping the catalytic zone (red area) compared to the C_3H_6 forming limits. The xC_3H_7O mechanism underpredicts $S(C_3H_6)$ by over 20% (- - -), while overpredicting $S(C_2H_4)$ by 6% (- - -) and both observed C_1 products slightly – this mechanism is the most selective towards CO (- - - , 2.4%). By contrast, in the undiluted case the xC_3H_7 mechanism underpredicts $S(C_3H_6)$ to a smaller degree (·····), and it predicts the correct amount of C_2H_4 (·····). However, the selectivity to propylene oxide (·····) is nearly double that of the other mechanisms studied, as the propyl radicals are clearly forming cC_3H_6O in the gas-phase upon desorption from the catalyst (red zone). Finally, upon dilution of the catalytic bed, both mechanisms converge towards the values predicted for the M1 and M2 mechanisms above as the gas-phase chemistry pushes the selectivities towards equilibrium. Both mechanisms also predict cC_3H_6O and C_2H_3CHO selectivities similar to the M1 and M2 mechanisms, with the xC_3H_7O pathways yielding the highest amount of CH_2O (2.8%).

3.5 Catalysis in the C–C scission limit

The final limit mechanism studied here is a two-step model leading to C_2H_4 and CH_3 formation via O*s*–mediated adsorption (M5), see Table 3. From the multitude of possible saturated, unsaturated, or oxygenated C–C scission products, we chose the above two to directly stimulate C_2H_4 and CH_4 production. We note that detailed heterogeneous microkinetic mechanisms for C_3 species that also include C_2 products are rather rare: the above mentioned mechanism for propane partial oxidation over rhodium[25] only contains desorption pathways for C_3H_8, CO, CO_2, and CH_4; the mechanism for propane ODH over vanadium oxide catalysts is more complete[26] but has, to our knowledge, not been

evaluated together with gas-phase chemistry.

When the surface chemistry is shifted completely towards C–C scission (-·-·-), the $S(C_2H_4)$ (-·-·-) and $S(CH_4)$ (-·-·-) calculated for the undiluted case exceed the experimental values. Tian et al.[28] suggested a catalytic C–C scission would lead to a 1:1 C_2:C_1 distribution in products while a higher ratio of 2:1 is observed experimentally in the undiluted case.[8] The authors proposed a catalytic CH_3-coupling process as a way of accounting for this discrepancy.[28] Here, we obtain an overall C_2:C_1 ratio of 1.67 with the C_3H_6 forming mechanism (M2) and 1.91 with the C–C scission mechanism (M5). In undiluted cases, catalytic C–C scission unsurprisingly leads to higher C_2:C_1 ratios than mechanisms without surface C–C bond scission, and the experimental C_2:C_1 ratios can be matched without CH_3-coupling surface reactions. In all other aspects, the C–C scission limit is very similar to the M3 mechanism corresponding to the xC_3H_7O forming limit (- - -). Upon dilution of the catalytic bed, a convergence with the other four mechanisms can be observed: significant underprediction in both $S(C_2H_4)$ (-·-·- , $\Delta = 5\%$) and $S(CO)$ (-·-·- , $\Delta = 8\%$), and a high selectivity to experimentally undetected products cC_3H_6O, C_2H_3CHO, and CH_2O.

3.6 Addressing gas-phase selectivity

The selectivity envelope of the limit surface mechanisms as well as the contribution of the gas-phase chemistry can be used to inform an initial heterogeneous model. First, we attempt to reconcile the selectivity towards propylene oxide calculated with the DTU mechanism with the observed experimental data. The propylene oxide decomposition pathways in the JetSurF mechanism are based on a mechanism of Lifshitz and Tamburu[29] derived from shock tube experiments on propylene oxide. The mechanism was later expanded by Burluka et al.[30] using flame speed data. The decomposition pathways of cC_3H_6O from this expanded mechanism are listed in Table 4. We note that the cC_3H_6O and C_2H_3CHO pathways are not directly coupled. When included into the DTU mechanism (denoted "DTU + B."), the selectivity profiles obtained when coupled with M2 at high bed dilutions barely change, as shown in Fig. 6. However, the conversion of propane goes down appreciably, from 18.5% with DTU to 16.7% with DTU + B. using the same surface chemistry. We note that the current models for decomposition of propylene oxide may suffer from the lack of direct experimental data; direct measurements of propylene oxide flame structure

and associated mechanism benchmarking have been presented by Knyazkov et al. only recently.[22]

Table 4: Propylene oxide decomposition pathways from Burluka et al.[30]

Reaction equation	**Pre-exponential** A (m, mol, s)	**T-dependency** β (–)	**Barrier** E_A (kJ/mol)
$cC_3H_6O \leftrightarrow C_2H_5 + HCO$	2.450×10^{13}	0.0	244.8
$cC_3H_6O \leftrightarrow CH_3CH_2CHO$	1.840×10^{14}	0.0	244.8
$cC_3H_6O \leftrightarrow CH_3 + CH_3CO$	4.540×10^{13}	0.0	250.6
$cC_3H_6O \leftrightarrow CH_3 + CH_2CHO$	2.450×10^{13}	0.0	245.9
$cC_3H_6O \leftrightarrow CH_3 + cC_2H_3O$	8.000×10^{15}	0.0	384.6
$cC_3H_6O \leftrightarrow CH_3C(O)CH_3$	1.010×10^{14}	0.0	250.4
$cC_3H_6O \leftrightarrow cC_3H_5O + H$	8.000×10^{15}	0.0	384.6
$cC_3H_6O + H \leftrightarrow cC_3H_5O + H_2$	5.540×10^{-4}	3.5	21.7
$cC_3H_6O + H \leftrightarrow cC_2H_4O + CH_3$	2.770×10^{-5}	3.5	21.7
$cC_3H_6O + O \leftrightarrow cC_3H_5O + OH$	7.200×10^{2}	1.56	35.5
$cC_3H_6O + OH \leftrightarrow cC_3H_5O + H_2O$	1.548×10^{1}	1.83	11.6
$cC_3H_6O + HO_2 \leftrightarrow cC_3H_5O + H_2O_2$	4.680×10^{-2}	2.5	87.8
$cC_3H_6O + CH_3 \leftrightarrow cC_3H_5O + CH_4$	1.000×10^{6}	0.0	41.8
$cC_3H_6O + CH_3OO \leftrightarrow cC_3H_5O + CH_3OOH$	1.810×10^{5}	0.0	77.2
$cC_3H_6O + cC_2H_3O \leftrightarrow cC_3H_5O + cC_2H_4O$	2.250×10^{-4}	3.65	38.0
$cC_3H_5O \leftrightarrow CH_2CO + CH_3$	1.510×10^{14}	0.0	250.4
$cC_3H_5O \leftrightarrow C_2H_4 + HCO$	2.450×10^{14}	0.0	244.5
$cC_3H_5O \leftrightarrow C_2H_3 + CH_2O$	3.240×10^{13}	0.0	244.5

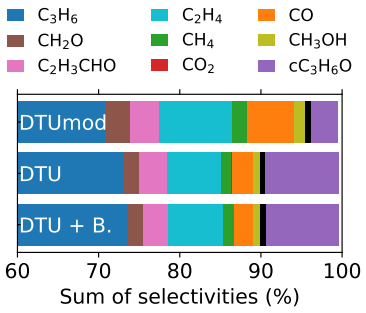

Figure 6: The effect of propylene oxide decomposition pathways on the selectivities. Shown for $V_{\text{bed}}/V_{\text{cat}} = 8.5$ at ~ 40 ml/min flow rate, with Os-mediated C_3H_6 forming mechanism (M2).

A different approach to address the cC_3H_6O issue is to augment the original DTU mechanism by scaled cC_3H_6O decomposition pathways, shown in Table 5. The pre-exponential of the two pathways was scaled by $\times 1000$ from the original values (cf. Table 4) so that $S(cC_3H_6O)$ is reduced to around 3%. A comparison of selectivities for the original DTU mechanism and this augmented mechanism is shown in Fig. 6 with the augmented mechanism denoted "DTUmod". Both gas-phase chemistries are again coupled to M2. The $S(cC_3H_6O)$ is significantly reduced (■, $\Delta = -5.8\%$), accompanied with

an appreciable reduction in $S(C_3H_6)$ (■, $\Delta = -2.3\%$). Upon inclusion of the two gas-phase C–C scission pathways, a significant increase in $S(C_2H_4)$ (■, $\Delta = +2.2\%$) and $S(CO)$ (■, $\Delta = +3.3\%$) is observed. Among the species that were not experimentally detected are formaldehyde (CH_2O, ■, $\Delta = +2.0\%$) and acrolein (C_2H_3CHO, ■, $\Delta = +2.7\%$) at 3.1% and 3.6% respectively. The modification of the DTU mechanism therefore improves the agreement with experiment significantly. However, given the unreasonable scaling of the rates of the gas-phase pathways required to reduce the selectivity to propylene oxide, a further investigation into the low temperature decomposition of propylene oxide in the gas-phase as well as on the surface is required to properly capture the evolution of minor species.

Table 5: Scaled propylene oxide decomposition pathways in DTUmod mechanism

Reaction equation	**Pre-exponential** A (m, mol, s)	**T-dependency** β (–)	**Barrier** E_A (kJ/mol)
$cC_3H_6O \leftrightarrow C_2H_5 + HCO$	2.450×10^{16}	0.0	244.8
$cC_3H_6O \leftrightarrow CH_3 + CH_2CHO$	2.450×10^{16}	0.0	245.9

3.7 Effect of higher flow rates

When the DTUmod mechanism is coupled with the O*s*-mediated C_3H_6 mechanism (M2, -·-· in Fig. 7), the experimental $X(C_3H_8)$ (●) and $S(C_3H_6)$ (●) are well predicted at all studied inlet flow rates and catalyst dilution ratios: the maximum absolute deviation Δ_{max} in $X(C_3H_8)$ is 3.3% ($V_{bed}/V_{cat} = 8.5$, 100 ml min^{-1}), and Δ_{max} in $S(C_3H_6)$ is 4.7% ($V_{bed}/V_{cat} = 2.0$, 140 ml min^{-1}). The selectivity to propylene is generally overpredicted at cases with high dilutions and high flow, likely as a consequence of the underprediction in conversion. All qualitative trends with increasing flow rates are well captured, with the exception of the slightly increasing $S(CH_4)$ (●) with increased flow rate in the undiluted case. The apparent underprediction of CH_4 at V_{bed}/V_{cat} of 1.0 and 2.0 may be within the uncertainty of the experiment, given the scatter in the $S(CH_4)$ data at $V_{bed}/V_{cat} = 2.0$. With increasing dilution of the bed, $S(CO)$ (●) as well as $S(C_2H_4)$ (●) are increasingly underpredicted, despite the inclusion of the scaled gas-phase cC_3H_6O decomposition pathways. The lack of CO selectivity in the modelled data at dilutions above 2.0 could be due to the production of other minor C_1 species. In the most diluted case ($V_{bed}/V_{cat} = 8.5$, 40 ml min^{-1}), the sum of $S(CO)$ (5.85%), $S(CH_2O)$ (3.09%), and $S(CH_3OH)$ (1.24%) is within 1% of the experimental $S(CO)$ (10.78%), implying the right total amount of C_1 oxygenated

products is formed. We refer the reader to Fig. 2, where we indicated the low-temperature oxidation behaviour of the DTU mechanism may be questionable.

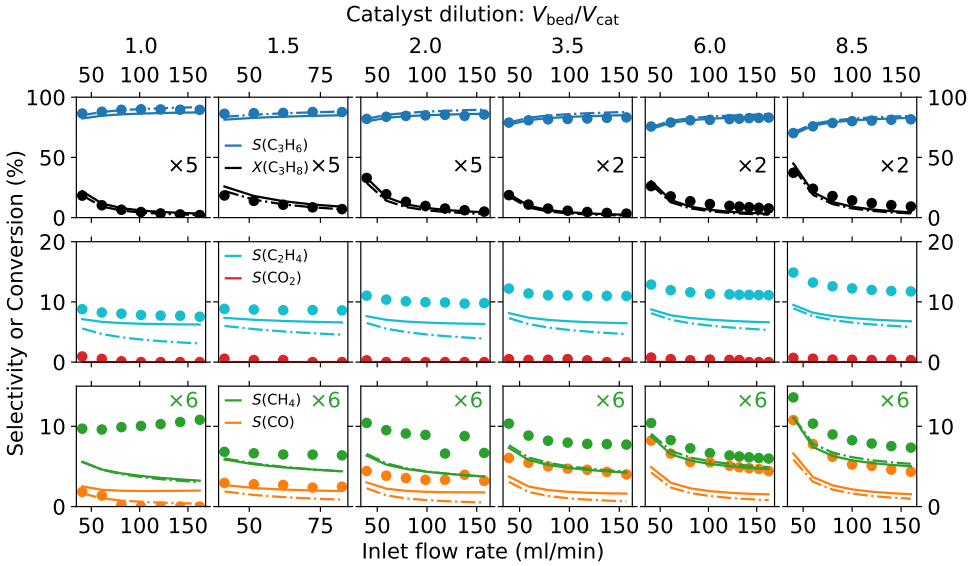

Figure 7: Selectivity and conversion of selected species as a function of inlet flow rate for all studied catalyst dilution ratios. Symbols are experimental data,[8] lines are results calculated with the DTUmod mechanism coupled to M2 (-·-·-), and the DTUmod mechanism coupled to a mechanism including C–C scission pathways (——).

3.8 Towards a predictive model

The agreement of the model with the selectivities to C_2H_4 and CH_4 observed in the undiluted cases can be improved by incorporating propoxy radical formation (M4) or C–C bond scission (M5) into the surface mechanism. One such mechanism is shown in Table 6. The base of this mechanism is the propane oxidation mechanism of Hartmann et al.[25] augmented by desorption pathways for ethylene. To reduce the numerical stiffness of the model, we have eliminated the Hs species and associated reactions from the H/O sub-mechanism, retaining only R4–R11 and R14 from Table 1. All steps shown in Table 6 are now accompanied by reverse pathways. The adsorption steps of C_3H_8, C_3H_6, C_2H_4, and CO are associative and adsorb on an empty site, while adsorption of CH_4 is dissociative and involves an Os site. With the exception of CO, all adsorption sticking coefficients are estimates. The propane s_0 is adjusted to match conversion analogously to the limit mechanisms above. The obtained propane sticking coefficient of 3.2×10^{-9} in R15-f is significantly lower than that on Rh ($s_0 = 5.8 \times 10^{-3}$),[25] a higher value would require adjusting the desorption barrier (R15-b), site density, and most likely the other

barriers as well as the H/O chemistry. Propylene and ethylene s_0's are set to 1.5× the s_0 of propane (R20-b and R21-b, respectively) and their desorption barriers (R20-f and R21-f) are set above that of propane due to the presence of a double bond as well as reduced steric interactions in ethylene. The dehydrogenation of C_3H_8s is assisted by Os and ultimately leads to C_3H_6s over two steps (R16-f, R17-f). Both intermediate products are allowed to undergo C–C scission forming C_2H_xs + CH_3s (R18-f, R19-f). The barriers of C_2H_7s scission (R18-f) and the reverse recombination (R18-b) are adjusted to properly capture selectivity towards C_2H_4. Finally, the surface C_1 chemistry consists of CH_3s desorption as methane following hydrogenation (R23-f) or as CO following several dehydrogenation steps (R24-f – R28-f). The hydrogenation pathway is adapted from Hartmann et al.[25] combining the hydrogenation and desorption steps into one. The latter pathway is also adapted from Hartmann et al.,[25] with CH_3O undergoing dehydrogenation instead of CH_3.

The results calculated with this mechanism coupled to the DTUmod gas-phase chemistry are shown in Fig. 7 (—). In the undiluted case, the incorporation of surface C–C scission helps to reproduce $S(C_2H_4)$ to within 1.7% at all flow rates (—), while $S(C_3H_6)$ is underpredicted only slightly ($\Delta = 4.1\%$, —) with the agreement improving as a function of flow. Selectivity to C_1 species at the lowest flow rate is comparable to the limit mechanism, however S(CO) (—) does not drop to zero at high flows. Due to the modifications of the gas-phase mechanism, $S(cC_3H_6O)$ is below 2.6% at all flow rates, i.e. within the error of the experimental mass balance.

The C–C scission mechanism is able to track the qualitative trends in all selectivities as a function of bed dilution and inlet flow rate – the only exception is the increase in $S(CH_4)$ as a function of flow in the undiluted case, also discussed above. The C–C scission mechanism also overpredicts $X(C_3H_8)$ (—) for all cases with inlet flow $\sim$ 40 ml min^{-1}. At intermediate dilutions ($V_{bed}/V_{cat} \leq 2.0$), the surface C–C scission chemistry leads to an improved agreement with experiment compared to the M2 mechanism in both S(CO) (—) as well as $S(C_2H_4)$ (—). At dilutions ≥ 3.5, the two products become increasingly more underpredicted ($\Delta = 5.4\%$ and 4.2% for C_2H_4 and CO, respectively). As with the M2 mechanism, the sum of calculated S(CO) (6.61%), $S(CH_2O)$ (3.17%), and $S(CH_3OH)$ (1.31%) is within 0.5% of the experimental S(CO) (10.78% at $V_{bed}/V_{cat} = 8.5$, 40 ml min^{-1}). Similarly, the calculated selectivity to propylene oxide (3.76%) and acrolein (3.25%) may be responsible for the underprediction in $S(C_2H_4)$.

Table 6: Heterogeneous C_3 submechanism including C–C scission.

Pathway	**Reaction equation**	**Pre-exponential** A (m, mol, s)	**T-dep.** β (–)	**Barrier** E_A (kJ/mol)	**Source**
R15-f	$C_3H_8 + Bs \rightarrow C_3H_8s$	$s_0 = 3.2 \times 10^{-9}$	–	–	fitted
R15-b	$C_3H_8s \rightarrow C_3H_8 + Bs$	1.3×10^{13}	0	30.1	Hartmann
R16-f	$C_3H_8s + Os \rightarrow C_3H_7s + OHs$	3.7×10^{21}	0	71.5	Hartmann
R16-b	$C_3H_7s + OHs \rightarrow C_3H_8s + Os$	3.7×10^{21}	0	31.3	Hartmann
R17-f	$C_3H_7s + Os \rightarrow C_3H_6s + OHs$	3.7×10^{21}	0	88.7	Hartmann
R17-b	$C_3H_6s + OHs \rightarrow C_3H_7s + Os$	3.7×10^{21}	0	45.3	Hartmann
R18-f	$C_3H_7s + Bs \rightarrow C_2H_4s + CH_3s$	3.7×10^{21}	0	80.0	fitted
R18-b	$C_2H_4s + CH_3s \rightarrow C_3H_7s + Bs$	3.7×10^{21}	0	46.0	fitted
R19-f	$C_3H_6s + Bs \rightarrow C_2H_3s + CH_3s$	3.7×10^{21}	0	83.7	Hartmann
R19-b	$C_2H_3s + CH_3s \rightarrow C_3H_6s + Bs$	3.7×10^{21}	0	55.8	Hartmann
R20-f	$C_3H_6s \rightarrow C_3H_6 + Bs$	1.3×10^{13}	0	45.0	estimate
R20-b	$C_3H_6 + Bs \rightarrow C_3H_6s$	$s_0 = 4.8 \times 10^{-9}$	–	–	estimate
R21-f	$C_2H_4s \rightarrow C_2H_4 + Bs$	1.3×10^{13}	0	55.0	estimate
R21-b	$C_2H_4 + Bs \rightarrow C_2H_4s$	$s_0 = 4.8 \times 10^{-9}$	–	–	estimate
R22-f	$C_2H_3s + OHs \rightarrow C_2H_4s + Os$	3.7×10^{21}	0	45.0	estimate
R22-b	$C_2H_4s + Os \rightarrow C_2H_3s + OHs$	3.7×10^{21}	0	90.0	estimate
R23-f	$CH_3s + OHs \rightarrow CH_4 + Os + Bs$	3.7×10^{21}	0	24.3	Hartmann
R23-b	$CH_4 + Os + Bs \rightarrow CH_3s + OHs$	$s_0 = 0.8 \times 10^{-9}$	–	–	estimate
R24-f	$CH_3s + Os \rightarrow CH_3Os + Bs$	3.7×10^{21}	0	56.0	estimate
R24-b	$CH_3O + Bs \rightarrow CH_3s + Os$	3.7×10^{21}	0	80.0	estimate
R25-f	$CH_3Os + Os \rightarrow CH_2Os + OHs$	3.7×10^{21}	0	103.0	Hartmann
R25-b	$CH_2Os + OHs \rightarrow CH_3Os + Os$	3.7×10^{21}	0	44.0	Hartmann
R26-f	$CH_2Os + Os \rightarrow CHOs + OHs$	3.7×10^{21}	0	100.0	Hartmann
R26-b	$CHOs + OHs \rightarrow CH_2Os + Os$	3.7×10^{21}	0	68.0	Hartmann
R27-f	$CHOs + Os \rightarrow COs + OHs$	3.7×10^{21}	0	21.0	Hartmann
R27-b	$COs + OHs \rightarrow CHOs + Os$	3.7×10^{21}	0	172.8	Hartmann
R28-f	$COs \rightarrow CO + Bs$	3.5×10^{13}	0	133.4 - $15\Theta_{CO_s}$	Hartmann
R28-b	$CO + Bs \rightarrow COs$	$s_0 = 0.5$	–	–	Hartmann

4 Summary and outlook

The current work proposes that gas-phase chemistry is the main driver of the catalytic performance of hBN as a selective catalyst for ODH of propane. The hBN surface acts as a driver of conversion, however the influence of the surface chemistry on the resulting product distribution decreases significantly with dilution of the catalytic bed, as gas-phase effects begin to dominate. The work highlights the necessity of modelling of the whole heated section of the reactor: even if little to no conversion is observed in blank experiments, and best practices to limit post-catalytic combustion are followed, we show the post-catalytic zone can be responsible for up to 50% of the total observed conversion.

The limit heterogeneous mechanisms applied in this work reveal that C_3H_6 is the main but likely not the only product desorbing from the catalytic surface. A contribution of catalytic C–C scission products is required to reproduce the experimentally observed 2:1 C_2:C_1 product ratio in undiluted beds. However, the correct selectivity to C_2H_4 in undiluted cases can be obtained without catalytic C–C scission, e.g. by xC_3H_7O desorption as a minor product. As a first step towards a predictive model, we have adapted the heterogeneous mechanism developed for propane oxidation over Rh,[25] and coupled it with the DTU gas-phase mechanism[9] augmented by scaled propylene oxide decomposition pathways. This combined mechanism yields a reasonable agreement in selectivities of major and minor products at all studied flows in catalytic bed dilution ratios ≤ 2.0. However, there is a substantial scope for further mechanism development in two key areas:

1. The H/O submechanism, which may play an important role in H-abstraction reactions. Further experimental data such as hydrogen selectivities in ODH or oxidation of H_2 would support such efforts greatly, such as the works of the groups of Deutschmann[31–33] or Mantzaras[34–36] on metals.

2. The rate constants of the $C_3/C_2/C_1$ submechanism. These rate constants can be in principle derived using semi-empirical[17,37] or ab initio methods,[38,39] however a wider range of reaction temperatures and inlet compositions is necessary to validate any such efforts.

The gas-phase chemistry is responsible for the majority of the catalytic behaviour observed in diluted beds. Conversion of propane and selectivity to propylene in particular converge towards the gas-phase values, regardless of the surface product distribution. However, the DTU mechanism[9] predicts the formation of a significant amount of propylene oxide, and to a lesser extent acrolein and formaldehyde. The overprediction of propylene oxide is most likely a mechanistic artefact due to missing decomposition pathways. While the C_3:C_2:C_1 product distribution predicted using the modified DTU mechanism matches the experimentally observed distribution, the detailed speciation, particularly of C_1 oxygenated species, is at odds with the modelled experiments. Further study of the low-temperature oxidation chemistry of the above species is necessary.

Finally, we would like to emphasise the importance of evaluating gas-phase kinetics in any mechanistic study involving heterogeneous phenomena at elevated temperatures. One of the key advantages of microkinetics over the Langmuir-Hinshelwood-Hougen-Watson model is the ease with which gas-phase

and heterogeneous models of various complexities can be coupled. With open-source solvers, such as Cantera,[10] the tools are available to everyone; we hope that the executable code archive attached in the Supporting information may encourage wider adoption of such approaches in the catalytic community.

Acknowledgment

PK would like to thank the Forrest Research Foundation for funding.

Supporting information

Supporting information available. The complete code archive including all calculations, parameter fitting, and plotting scripts is available on Zenodo under DOI: 10.5281/zenodo.4106081. The archive is arranged in a Binder-executable format, see `https://mybinder.org/v2/zenodo/10.5281/zenodo.4106081/?filepath=index.ipynb`

References

[1] J. T. Grant, C. A. Carrero, F. Goeltl, J. Venegas, P. Mueller, S. P. Burt, S. E. Specht, W. P. McDermott, A. Chieregato, and I. Hermans, "Selective oxidative dehydrogenation of propane to propene using boron nitride catalysts," Science, vol. 354, pp. 1570–1573, Dec. 2016.

[2] L. Shi, D. Wang, W. Song, D. Shao, W.-P. Zhang, and A.-H. Lu, "Edge-hydroxylated boron nitride for oxidative dehydrogenation of propane to propylene," ChemCatChem, vol. 9, pp. 1788–1793, May 2017.

[3] C. A. Carrero, R. Schloegl, I. E. Wachs, and R. Schomaecker, "Critical literature review of the kinetics for the oxidative dehydrogenation of propane over well-defined supported vanadium oxide catalysts," ACS Catal., vol. 4, pp. 3357–3380, Oct. 2014.

[4] P. Chaturbedy, M. Ahamed, and M. Eswaramoorthy, "Oxidative dehydrogenation of propane over a high surface area boron nitride catalyst: Exceptional selectivity for olefins at high conversion," ACS Omega, vol. 3, pp. 369–374, Jan. 2018.

[5] J. T. Grant, W. P. McDermott, J. M. Venegas, S. P. Burt, J. Micka, S. P. Phivilay, C. A. Carrero, and I. Hermans, "Boron and boron-containing catalysts for the oxidative dehydrogenation of propane," ChemCatChem, vol. 9, pp. 3623–3626, Oct. 2017.

[6] J. M. Venegas and I. Hermans, "The influence of reactor parameters on the boron nitride-catalyzed oxidative dehydrogenation of propane," Org. Process Res. Dev., vol. 22, pp. 1644–1652, Dec. 2018.

[7] L. Shi, D. Wang, and A.-H. Lu, "A viewpoint on catalytic origin of boron nitride in oxidative dehydrogenation of light alkanes," Chinese Journal of Catalysis, vol. 39, pp. 908–913, May 2018.

[8] J. M. Venegas, W. P. McDermott, and I. Hermans, "Serendipity in Catalysis Research: Boron-Based Materials for Alkane Oxidative Dehydrogenation," Acc. Chem. Res., vol. 51, pp. 2556–2564, Oct. 2018.

[9] H. Hashemi, J. M. Christensen, L. B. Harding, S. J. Klippenstein, and P. Glarborg, "High-pressure oxidation of propane," Proceedings of the Combustion Institute, vol. 37, no. 1, pp. 461–468, 2019.

[10] D. G. Goodwin, R. L. Speth, H. K. Moffat, and B. W. Weber, "Cantera: An object-oriented software toolkit for chemical kinetics, thermodynamics, and transport processes." Zenodo, Aug. 2018.

[11] H. Wang, E. Dames, B. Sirjean, D. A. Sheen, R. Tango, A. Violi, J. Y. W. Lai, F. N. Egolfopoulos, D. F. Davidson, R. K. Hanson, C. T. Bowman, C. K. Law, W. Tsang, N. P. Cernansky, D. L. Miller, and R. P. Lindstedt, "A high-temperature chemical kinetic model of n-alkane (up to n-dodecane), cyclohexane, and methyl-, ethyl-, n-propyl and n-butyl-cyclohexane oxidation at high temperatures, JetSurF version 2.0," Sept. 2010.

[12] C. F. Goldsmith, W. H. Green, and S. J. Klippenstein, "Role of O_2 + QOOH in low-temperature ignition of propane. 1. Temperature and pressure dependent rate coefficients," J. Phys. Chem. A, vol. 116, pp. 3325–3346, Apr. 2012.

[13] R. Sivaramakrishnan, M.-C. Su, J. V. Michael, S. J. Klippenstein, L. B. Harding, and B. Ruscic, "Shock Tube and Theoretical Studies on the Thermal Decomposition of Propane: Evidence for a Roaming Radical Channel," J. Phys. Chem. A, vol. 115, pp. 3366–3379, Apr. 2011.

[14] R. Sivaramakrishnan, N. Srinivasan, M.-C. Su, and J. Michael, "High temperature rate constants for OH+ alkanes," Proceedings of the Combustion Institute, vol. 32, no. 1, pp. 107–114, 2009.

[15] H. Wang, X. You, A. V. Joshi, S. G. Davis, A. Laskin, F. N. Egolfopoulos, and C. K. Law, "USC Mech Version II. High-temperature combustion reaction model of H_2/CO/C_1-C_4 compounds.," May 2007.

[16] O. Deutschmann, R. Schmidt, F. Behrendt, J. Warnatz, and J. Warnat, "Numerical modeling of catalytic ignition," Proc. Combust. Inst., vol. 26, no. 1, pp. 1747–1754, 1996.

[17] P. Kraus and R. P. Lindstedt, "Microkinetic mechanisms for partial oxidation of methane over platinum and rhodium," J. Phys. Chem. C, vol. 121, pp. 9442–9453, May 2017.

[18] V. R. Tarnawski, T. Momose, and W. H. Leong, "Thermal conductivity of standard sands II. Saturated conditions," Int J Thermophys, vol. 32, pp. 984–1005, May 2011.

[19] S. L. Shindé and J. Goela, High Thermal Conductivity Materials. New York: Springer, 2006.

[20] G. Magnani, S. Galvagno, G. Sico, S. Portofino, C. Freda, and E. Burresi, "Sintering and mechanical properties of *B*-SiC powder obtained from waste tires," J Adv Ceram, vol. 5, pp. 40–46, Mar. 2016.

[21] J. A. Loiland, Z. Zhao, A. Patel, and P. Hazin, "Boron-containing catalysts for the oxidative dehydrogenation of ethane/propane mixtures," Ind. Eng. Chem. Res., vol. 58, pp. 2170–2180, Feb. 2019.

[22] D. A. Knyazkov, A. M. Dmitriev, O. P. Korobeinichev, K. N. Osipova, G. Pio, A. G. Shmakov, and E. Salzano, "Structure of premixed flames of propylene oxide: Molecular beam mass spectrometric study and numerical simulation," Proceedings of the Combustion Institute, p. S1540748920304296, Sept. 2020.

[23] Z. Kalenik and E. E. Wolf, "The role of gas-phase reactions during methane oxidative coupling," in Methane Conversion by Oxidative Processes: Fundamental and Engineering Aspects, Van Nostrand Reinhold Catalysis Series, p. 548, Springer Science & Business Media, 2013.

[24] G. Shangpeng, "Crystal structures and band gap characters of h-BN polytypes predicted by the dispersion corrected DFT and GW method," Solid State Communications, vol. 152, pp. 1817–1820, 2012.

[25] M. Hartmann, L. Maier, H. Minh, and O. Deutschmann, "Catalytic partial oxidation of iso-octane over rhodium catalysts: An experimental, modeling, and simulation study," Combustion and Flame, vol. 157, pp. 1771–1782, Sept. 2010.

[26] X. Rozanska, R. Fortrie, and J. Sauer, "Oxidative Dehydrogenation of Propane by Monomeric Vanadium Oxide Sites on Silica Support," J. Phys. Chem. C, vol. 111, pp. 6041–6050, Apr. 2007.

[27] L. Shi, Y. Wang, B. Yan, W. Song, D. Shao, and A.-H. Lu, "Progress in selective oxidative dehydrogenation of light alkanes to olefins promoted by boron nitride catalysts," Chem. Commun., vol. 54, no. 78, pp. 10936–10946, 2018.

[28] J. Tian, J. Tan, M. Xu, Z. Zhang, S. Wan, S. Wang, J. Lin, and Y. Wang, "Propane oxidative dehydrogenation over highly selective hexagonal boron nitride catalysts: The role of oxidative coupling of methyl," Sci. Adv., vol. 5, p. eaav8063, Mar. 2019.

[29] A. Lifshitz and C. Tamburu, "Isomerization and decomposition of propylene oxide. Studies with a single-pulse shock tube," J. Phys. Chem., vol. 98, pp. 1161–1170, Jan. 1994.

[30] A. Burluka, M. Harker, H. Osman, C. Sheppard, and A. Konnov, "Laminar burning velocities of three C_3H_6O isomers at atmospheric pressure," Fuel, vol. 89, pp. 2864–2872, Oct. 2010.

[31] C. Karakaya and O. Deutschmann, "Kinetics of hydrogen oxidation on Rh/Al2O3 catalysts studied in a stagnation-flow reactor," Chemical Engineering Science, vol. 89, pp. 171–184, Feb. 2013.

[32] H. Karadeniz, C. Karakaya, S. Tischer, and O. Deutschmann, "Numerical modeling of stagnation-flows on porous catalytic surfaces: CO oxidation on Rh/Al2O3," Chemical Engineering Science, vol. 117, pp. 136–136, 2014.

[33] C. Karakaya, H. Karadeniz, L. Maier, and O. Deutschmann, "Surface Reaction Kinetics of the Oxidation and Reforming of Propane over Rh/Al $_2$ O $_3$ Catalysts," ChemCatChem, vol. 9, pp. 685–695, Feb. 2017.

[34] M. Reinke, J. Mantzaras, R. Schaeren, R. Bombach, A. Inauen, and S. Schenker, "High-pressure catalytic combustion of methane over platinum: In situ experiments and detailed numerical predictions," Combustion and Flame, vol. 136, pp. 217–240, Jan. 2004.

[35] X. Zheng, J. Mantzaras, and R. Bombach, "Kinetic interactions between hydrogen and carbon monoxide oxidation over platinum," Combustion and Flame, vol. 161, pp. 332–346, Jan. 2014.

[36] R. Sui, J. Mantzaras, and R. Bombach, "A comparative experimental and numerical investigation of the heterogeneous and homogeneous combustion characteristics of fuel-rich methane mixtures over rhodium and platinum," Proceedings of the Combustion Institute, vol. 36, no. 3, pp. 4313–4320, 2017.

[37] M. Maestri, D. Livio, A. Beretta, and G. Groppi, "Hierarchical Refinement of Microkinetic Models: Assessment of the Role of the WGS and r-WGS Pathways in CH $_4$ Partial Oxidation on Rh," Ind. Eng. Chem. Res., vol. 53, pp. 10914–10928, July 2014.

[38] M. A. Christiansen, G. Mpourmpakis, and D. G. Vlachos, "DFT-driven multi-site microkinetic modeling of ethanol conversion to ethylene and diethyl ether on γ-Al2O3(1 1 1)," Journal of Catalysis, vol. 323, pp. 121–131, Mar. 2015.

[39] P. Kraus and I. Frank, "Constrained chemical dynamics of CO dissociation/hydrogenation on Rh surfaces," Chem. Eur. J., vol. 24, pp. 7188–7199, May 2018.